Acta Crystallographica Section B
Structural Science
ISSN 0108-7681

Chemical bonding in pentaerythritol at very low temperature or at high pressure: an experimental and theoretical study

Elizabeth A. Zhurova,[a] Vladimir G. Tsirelson,[b] Vladimir V. Zhurov,[a,c] Adam I. Stash[c] and A. Alan Pinkerton[a]*

[a]Department of Chemistry, University of Toledo, Toledo, OH 43606, USA, [b]Mendeleev University of Chemical Technology, Moscow, Russia, and [c]Karpov Institute of Physical Chemistry, Moscow, Russia

Correspondence e-mail: apinker@uoft02.utoledo.edu

Received 1 November 2005
Accepted 6 March 2006

Chemical bonding in the pentaerythritol crystal based on the experimental electron density at 15 (1) K, and theoretical calculations at the experimental molecular geometries obtained at room and low (15 K) temperatures have been analyzed and compared in terms of the topological analysis. Topological electron-density features corresponding to the high-pressure (1.15 GPa) geometry are also reported. In addition to the bond critical points (CPs) within the molecular layers, CPs between the atoms of different molecular layers have been located and the bonding character of these relatively weak interactions discussed. Atomic charges and energies have been integrated over the atomic basins delimited by the zero-flux surfaces, and the intermolecular interaction energies have been calculated. The interaction between molecular layers in the crystal becomes stronger both at very low temperature and high pressure, as demonstrated by the more negative intermolecular interaction energies, higher electron density and energy density values at the CPs, and sharper electronic-energy density profiles.

1. Introduction

In order to gain insight into the properties of energetic materials (explosives, propellants), we have initiated a program to obtain their electronic properties derived from experimental and theoretical electron-density distributions. Our studies to date have been limited to crystalline solids at low temperature and ambient pressure (Zhurova & Pinkerton, 2001; Zhurova, Tsirelson, Stash & Pinkerton, 2002; Zhurova, Martin & Pinkerton, 2002; Ritchie *et al.*, 2003; Pinkerton *et al.*, 2003; Zhurova *et al.*, 2004). Clearly, there would be much interest in obtaining similar information at the higher pressures developed during explosions or propellant burning. Unfortunately, the quality of X-ray diffraction data from crystals under pressure is currently inadequate for this purpose. Therefore, an appropriate theoretical calculation based on structural parameters obtained under pressure may provide the desired bonding information. To test this hypothesis, we have carried out a benchmark study on pentaerythritol, $C_5H_{12}O_4$: we have compared theory and experiment at low temperature to validate the theoretical results and then compared three theoretical studies based on structural data obtained under ambient conditions and at low temperature or high pressure.

Pentaerythritol [2,2-bis(hydroxymethyl)-1,3-propanediol], whose crystal structure at ambient conditions (Llewellyn *et al.*, 1937; Ladd, 1979; Eilerman & Rudman, 1979; Semmingsen, 1988) as well as at high pressure (Katrusiak, 1995) and low temperature (Zhurov *et al.*, 2005) has been previously reported, is a good candidate for such a study. The penta-

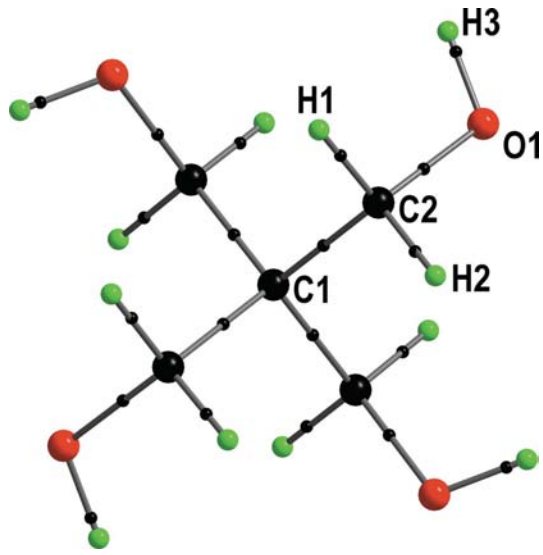

Figure 1
Pentaerythritol molecule with intramolecular CPs shown as small black balls.

erythritol molecule (Fig. 1) consists of four C—CH_2—OH fragments with the C2 atoms forming an almost ideal tetrahedron around C1, slightly elongated along the crystallographic *c*-axis direction (Katrusiak, 1995). The compound crystallizes in space group $I\bar{4}$ at temperatures up to 452.7 K and no evidence of a pressure-induced phase transition has been reported (Katrusiak, 1995). Crystalline pentaerythritol has a small unit cell with a 1/4 molecule in the asymmetric unit and is built of sheets of hydrogen-bonded molecules (Fig. 2). Since pentaerythritol is a prototype crystal for the explosive pentaerythritol tetranitrate (PETN), we propose to determine to what extent the atomic interactions change in these two compounds with respect to temperature and pressure. As a first step, in this paper we present the study of bonding in pentaerythritol, based on the experimental electron density derived from our X-ray diffraction data measured at 15 K (Zhurov *et al.*, 2005). We also report similar results from several theoretical calculations based on the crystal structures with geometrical parameters corresponding to two different temperatures and high pressure.

2. Experimental measurements and theoretical calculations

The X-ray diffraction experiment was performed using a Rigaku R-Axis rapid diffractometer with a high-power Mo rotating-anode generator (18 kW), graphite monochromator and a curved image-plate detector, with cooling to 15 (1) K provided by an open-flow helium cryostat (Hardie *et al.*, 1998; Kirschbaum *et al.*, 1999; Ribaud *et al.*, 2001). The experimental details have been published elsewhere (Zhurov *et al.*, 2005). In summary, 295 diffraction patterns providing 27 057 reflections were measured; they were reduced to 2378 independent reflections (R_{merge} = 0.0183) with $\sin\theta/\lambda \leq 1.323$ Å^{-1}. The experimental results are referred to in Tables 1–3 as (I).[1]

Theoretical calculations of the crystalline pentaerythritol (DFT/B3LYP, 6-311G**) have been performed at different fixed experimental geometries with the *CRYSTAL*98 program (Saunders *et al.*, 1998). First, atomic coordinates derived from our experimental data at 15 K were used; this calculation will be referred to as the 'low-temperature' calculation [(II) in Tables 1–4]. Second, the atomic coordinates and the unit-cell

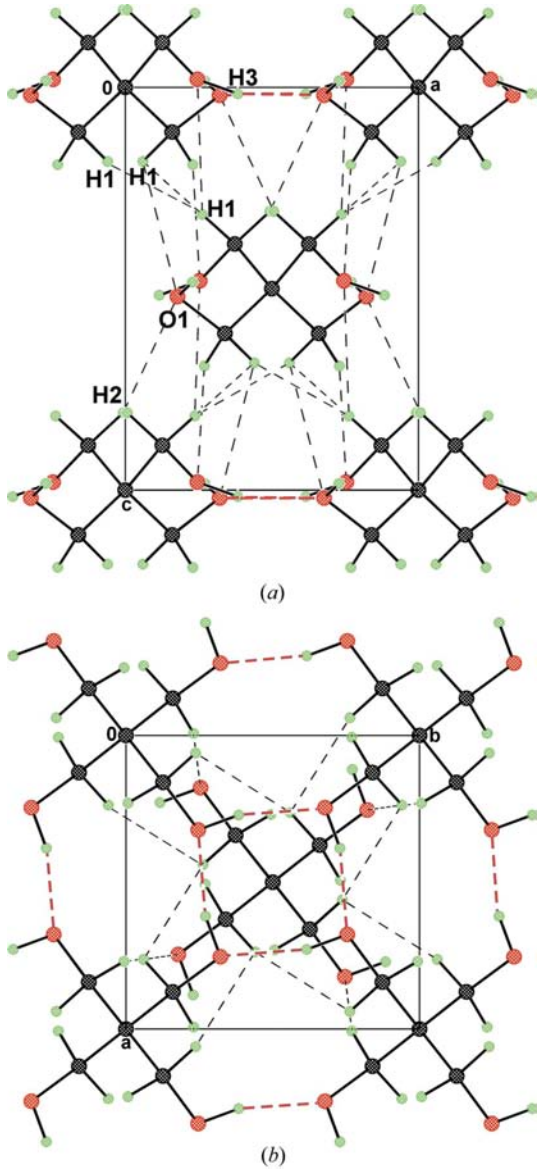

Figure 2
Molecular packing in the pentaerythritol crystal at 1.15 GPa: (*a*) projection down the *b* axis; (*b*) projection down the *c* axis. O atoms are red, C atoms are black and H atoms are green. Red dashed lines represent 'classical' (short) hydrogen bonding within the molecular layers and black dashed lines depict weaker (longer) contacts corresponding to observed bond paths in the electron density.

[1] Supplementary data for this paper are available from the IUCr electronic archives (Reference: LB5001). Services for accessing these data are described at the back of the journal.

Table 1
Data treatment details and intra- and intermolecular bond distances (°).

	(I) Expt., low temp. atm. pressure	(II) Theory, low temp. atm. pressure	(III) Theory, room temp. atm. pressure	(IV) Theory, room temp. high pressure
Data refinement				
$R(F)$	0.0118	0.0041	0.0039	0.0041
No. of parameters	115	92	92	92
No. of reflections	2378	1307	1307	1307
$\sin(\theta/\lambda)_{max}$ (Å^{-1})	1.323	1.000	1.000	1.000
Space group	$I\bar{4}$	$I\bar{4}$	$I\bar{4}$	$I\bar{4}$
a (Å)	6.0867 (1)	6.0867	6.079 (3)†	6.017 (1)‡
c (Å)	8.4958 (4)	8.4958	8.745 (4)†	8.267 (3)‡
V (Å)	314.75	314.75	323.16	299.30
Bond/interatomic distances				
C1—C2	1.5348 (1)	1.5348	1.529 (2)†	1.533 (3)‡
C2—O1	1.4273 (2)	1.4273	1.422 (3)†	1.427 (4)‡
C2—H1	1.081	1.081	1.081 (6)†	1.081
C2—H2	1.070	1.070	1.070 (6)†	1.070
O1—H3	0.933	0.933	0.933 (6)†	0.933
O1···H3§	1.7994	1.7994	1.790	1.777
C1···C1¶	6.047	6.047	6.132	5.932

† Taken from the neutron diffraction study (Semmingsen, 1988). ‡ Taken from the X-ray diffraction study at 1.15 GPa (Katrusiak, 1995). § Hydrogen bonds within molecular sheets. ¶ C1 at (0, 0, 0) and C1 at $(\frac{1}{2}, \frac{1}{2}, \frac{1}{2})$.

parameters were taken from a neutron diffraction study (Semmingsen, 1988) performed at room temperature (294 K) and normal pressure [referred to as the 'room-temperature' calculation, (III)]. Finally, the atomic coordinates and unit-cell parameters were taken from the reported X-ray diffraction study (Katrusiak, 1995) at room temperature and 1.15 GPa pressure [referred as the 'high-pressure' calculation (IV)]. Since X-ray diffraction experiments do not provide accurate positions of the H atoms, in cases (II) and (IV) the C—H and O—H distances were fixed to the neutron values derived at normal pressure and room temperature [(III), see Table 1]. Structure factors for all non-forbidden reflections in the space group $I\bar{4}$ up to $\sin\theta/\lambda = 1.0$ Å^{-1} were then generated and a multipole model (Hansen & Coppens, 1978) was refined over these three theoretical data sets, as well as over the experimental data with the *XD* program (Koritsanszky *et al.*, 2003). For the O and C atoms the multipole refinement was performed up to the hexadecapole level and for H atoms up to the quadrupole level. Only multipole model parameters were refined for the theoretical data, whereas for the experimental data, atomic coordinates, displacement parameters and a scale factor have been refined as well. The molecular electroneutrality condition was imposed throughout all the refinements. In all the refinements, the C—H and O—H bond lengths were fixed to the reported neutron values (Semmingsen, 1988; Table 1). In the experimental case, refinement of the radial expansion/contraction parameters for the H atoms did not improve either the R value or the model, therefore, $\kappa = \kappa' = 1.2$ were taken and fixed in this case. In the refinements over the theoretical structure factors, the κ and κ' values were refined for all atoms, including the H atoms. In each case, the ratios of observed and calculated structure factors averaged over 0.05 Å^{-1} intervals appeared to be very close to unity (Zhurov *et al.*, 2005), indicating a correct scale factor for all data (experimental case), as well as a well fitting model for the whole $\sin\theta/\lambda$ range. The residual experimental electron density showed no significant features more than ± 0.06 e Å^{-3} (Zhurov *et al.*, 2005). The condition of the total electron density being non-negative everywhere in space was fulfilled in all cases. Other refinement details are listed in Table 1 and the multipole model parameters for all four refinements have been deposited. All analyses of the electron density as well as the atomic properties integrations were performed with the modified program *WinXPRO* (Stash & Tsirelson, 2002, 2005).

3. Results and discussion

We found that the static deformation electron-density maps ($\delta\rho_{mult} = \rho_{mult} - \rho_{sph}$, Fig. 3), as well as the Laplacians of the electron density (Fig. 4) are very similar for all four cases, therefore, only experimental and high-pressure geometry maps are shown. The electron concentrations associated with the intramolecular covalent bonds as well as the oxygen electron lone-pair regions are clearly seen in Fig. 4, as expected.

Properties at the CPs in the electron density (Bader, 1990) are listed in Table 2. For the closed-shell interactions, the kinetic (g), potential (v) and total electronic (h_e) energies at the CPs have also been calculated from the electron density and its derivatives using the DFT formulae and the local virial theorem for equilibrium structures (Kirzhnits, 1957; Abramov, 1997; Tsirelson, 2002; Espinosa, *et al.*, 1998, 1999; Espinosa & Molins, 2000). For the hydrogen bonds the dissociation energies have been calculated as $D_e = -v/2$ a.u. (Espinosa & Molins, 2000). We must specify that Bader's theory is applicable to equilibrium structures only, while the high-pressure geometrical parameters from Katrusiak (1995) do not necessarily correspond to a minimum on the potential-energy surface of crystalline pentaerythritol. Thus, we approximate the real pentaerythritol crystal under pressure with an equilibrium crystalline analogue having the same geometry. The AIM theory (Bader, 1990) is completely applicable to this structure, while the electron density and electronic energy features are still close to ones in the pentaerythritol crystal under pressure.

Inspection of Table 2 shows that the experimental electron density values for the C—C and C—O bonds are systematically higher than the theoretical ones, while the opposite picture is observed for C—H bonds and the hydrogen bonds.

Table 2
Bond critical points in the electron density.

Bond	ρ (e Å^{-3})	$\nabla^2\rho$ (e Å^{-5})	R_{ij} (Å)	d_1 (Å)	d_2 (Å)	λ_1 (e Å^{-5})	λ_2 (e Å^{-5})	λ_3 (e Å^{-5})	g (a.u.)	v (a.u.)	h_e (a.u.)	De (kJ mol^{-1})
(I) Experiment, low temperature, ambient pressure												
C1—C2	1.651	−10.23	1.535	0.731	0.804	−11.731	−10.842	12.345	–	–	–	–
C2—O1	1.858	−13.01	1.427	0.616	0.812	−15.423	−14.772	17.186	–	–	–	–
C2—H1	1.967	−20.95	1.081	0.706	0.375	−20.214	−18.957	18.222	–	–	–	–
C2—H2	1.977	−20.19	1.070	0.695	0.376	−20.258	−18.692	18.759	–	–	–	–
O1—H3	2.491	−39.63	0.933	0.725	0.208	−43.137	−39.382	42.889	–	–	–	–
O1···H3	0.224	3.18	1.799	1.156	0.645	−1.544	−1.098	5.825	0.0319	−0.0308	0.0011	40.39
O1···H1	0.023	0.36	2.942	1.680	1.412	−0.065	−0.037	0.466	0.0027	−0.0017	0.0010	2.21
O1···H2	0.028	0.44	2.804	1.652	1.160	−0.086	−0.040	0.564	0.0033	−0.0021	0.0012	2.79
H1···H1	0.014	0.22	2.617	1.369	1.435	−0.041	−0.017	0.277	0.0016	−0.0010	0.0007	–
(II) Theory, low temperature, ambient-pressure geometry												
C1—C2	1.601	−8.46	1.535	0.727	0.808	−10.516	−9.931	11.983	–	–	–	–
C2—O1	1.736	−11.54	1.427	0.608	0.820	−13.699	−13.198	15.356	–	–	–	–
C2—H1	2.018	−23.61	1.081	0.702	0.379	−20.337	−19.371	16.096	–	–	–	–
C2—H2	2.066	−26.01	1.070	0.695	0.375	−21.376	−20.096	15.457	–	–	–	–
O1—H3	2.586	−55.63	0.933	0.734	0.199	−46.375	−44.452	35.194	–	–	–	–
O1···H3	0.245	2.37	1.799	1.157	0.646	−1.515	−1.375	5.257	0.0278	−0.0310	−0.0032	40.69
O1···H1	0.025	0.38	2.942	1.653	1.317	−0.068	−0.035	0.482	0.0029	−0.0018	0.0011	2.39
H2···H2	0.036	0.40	2.469	1.187	1.318	−0.109	−0.069	0.575	0.0032	−0.0023	0.0009	–
H1···H1	0.022	0.25	2.617	1.313	1.304	−0.060	−0.051	0.362	0.0020	−0.0013	0.0007	–
(III) Theory, room temperature, ambient-pressure geometry												
C1—C2	1.615	−8.42	1.529	0.720	0.809	−10.590	−9.940	12.114	–	–	–	–
C2—O1	1.766	−12.43	1.422	0.605	0.817	−14.119	−13.520	15.210	–	–	–	–
C2—H1	2.022	−23.80	1.081	0.702	0.379	−20.457	−19.510	16.169	–	–	–	–
C2—H2	2.079	−26.34	1.070	0.696	0.374	−21.704	−20.347	15.706	–	–	–	–
O1—H3	2.585	−55.06	0.933	0.733	0.200	−46.310	−44.334	35.582	–	–	–	–
O1···H3	0.251	2.40	1.790	1.152	0.641	−1.572	−1.419	5.391	0.0285	−0.0321	−0.0036	42.09
O1···H1	0.019	0.28	3.087	1.717	1.399	−0.047	−0.024	0.352	0.0021	−0.0013	0.0008	1.69
H2···H2	0.031	0.33	2.563	1.233	1.359	−0.087	−0.067	0.484	0.0026	−0.0019	0.0008	–
H1···H1	0.020	0.23	2.665	1.340	1.325	−0.052	−0.043	0.322	0.0017	−0.0011	0.0006	–
(IV) Theory, room temperature, high-pressure geometry												
C1—C2	1.609	−8.28	1.533	0.725	0.808	−10.534	−9.940	12.190	–	–	–	–
C2—O1	1.721	−10.90	1.427	0.608	0.819	−13.563	−13.011	15.676	–	–	–	–
C2—H1	2.026	−23.78	1.081	0.698	0.383	−20.135	−19.369	15.721	–	–	–	–
C2—H2	2.066	−26.20	1.070	0.693	0.377	−21.640	−19.712	15.148	–	–	–	–
O1—H3	2.542	−54.70	0.933	0.736	0.197	−45.393	−43.438	34.126	–	–	–	–
O1···H3	0.260	2.61	1.777	1.144	0.635	−1.608	−1.407	5.630	0.0307	−0.0343	−0.0036	45.01
O1···H1	0.032	0.49	2.866	1.637	1.354	−0.094	−0.019	0.607	0.0038	−0.0025	0.0013	3.27
O1···H2	0.047	0.55	2.633	1.538	1.111	−0.175	−0.079	0.806	0.0046	−0.0034	0.0012	4.45
H1···H1	0.028	0.29	2.540	1.256	1.285	−0.081	−0.065	0.440	0.0023	−0.0016	0.0007	–

ρ is the electron density; $\nabla^2\rho$ is the Laplacian; R_{ij} is interatomic distance, d_1 and d_2 are the distances from the critical point to atoms 1 and 2, λ_1, λ_2, λ_3 are principle curvatures, g, v and h_e are the kinetic, potential and total electronic energies at the critical point, respectively, D_e is the dissociation energy calculated as $D_e = -v/2$ (a.u.) (Espinosa & Molins, 2000).

Among the theoretical results, the properties for the intramolecular bonds are very similar.[2] Experimentally, the C2—O1 bond distance becomes slightly longer at low temperature and high pressure (Table 1); theory suggests that the electron density at the corresponding CP is also lower under these conditions (Table 2). Although it is important to recognize that the experimental and theoretical results are not identical, they are still in good agreement. However, for subtle trends we prefer to compare values obtained from theory, thus avoiding effects due to the different source of structure factors.

Table 3 lists the atomic volumes, charges, and total electronic energies for all four models integrated over the atomic basins delimited by the zero-flux surfaces. The integrated Lagrangian [$L = -1/4\nabla^2\rho(\mathbf{r})$] for every atom was reasonably small, demonstrating the accuracy of the integration. All the atomic charges sum to small non-zero values; this confirms that the molecule is practically electroneutral, as required. The sums of atomic volumes reproduce the unit-cell volume per molecule with a maximum error of 0.3%. We have also calculated the atomic charges and volumes for procrystals using zero-flux surface partitioning (Maslen & Spackman, 1985; Zhurova, Tsirelson, Stash & Pinkerton, 2002). For the O and H atoms, the procrystal 'atomic charges' are far from zero, with the hydrogen charges being highly positive. The differences between these charges, $\delta q = q_{\rm AIM} - q^{\rm pro}_{\rm AIM}$ ('deformation charges'), reflect the interatomic electron transfer which accompanies the molecule and crystal formation. In the same way, the differences in atomic volumes, $\delta\Omega$, reflect how the atomic volumes change after the formation of the molecule or

[2] A different picture has been found in a theoretical study of solid CO_2 (Gracia *et al.*, 2004), however, we note that the pressures used were much higher than in the present study and that six different pressure-dependent phases were studied.

Table 3
Atomic charges (q), volumes (Ω) and total electronic energies (H_e) integrated over atomic basins.

Atom	q (e$^-$)	$q^{\rm promol}$ (e$^-$)	δq (e$^-$)	Ω (Å^3)	$\Omega^{\rm promol}$ (Å^3)	$\delta\Omega$ (Å^3)	$-H_e$ (a.u.)
(I) Experiment, low temperature, ambient pressure							
O1	−1.023	−0.722	−0.301	15.590	13.340	2.250	75.9334
C1	0.172	−0.001	0.173	5.739	6.427	−0.688	38.4478
C2	0.358	0.020	0.338	7.259	9.042	−1.783	38.1640
H1	0.076	0.132	−0.056	6.715	6.523	0.192	0.6314
H2	−0.006	0.135	−0.141	6.194	5.767	0.427	0.6824
H3	0.554	0.438	0.116	2.036	2.993	−0.957	0.3168
Molecule	0.009	0.006	0.003	156.918	157.085	−0.167	501.3591
$L_{\rm err}^{\rm molecule}$ = 0.00045 a.u., $L_{\rm err}^{\rm promolecule}$ = 0.00049 a.u., $\Omega_{\rm unit\ cell}/2$ = 157.376 Å^3, $H_e^{\rm Crystal98}$ = −498.5272 a.u.							
(II) Theory, low temperature, ambient pressure							
O1	−0.992	−0.722	−0.270	15.330	13.340	1.990	75.7252
C1	0.089	−0.001	0.090	5.986	6.427	−0.441	38.4753
C2	0.380	0.020	0.360	7.025	9.042	−2.017	38.0745
H1	−0.002	0.132	−0.134	7.078	6.523	0.555	0.6503
H2	0.013	0.135	−0.122	6.379	5.767	0.612	0.6460
H3	0.582	0.438	0.144	1.910	2.993	−1.083	0.2909
Molecule	0.010	0.006	0.004	156.876	157.085	−0.209	500.0225
$L_{\rm err}^{\rm molecule}$ = 0.00094 a.u., $L_{\rm err}^{\rm promolecule}$ = 0.00049 a.u., $\Omega_{\rm unit\ cell}/2$ = 157.376 Å^3, $H_e^{\rm Crystal98}$ = −498.5272 a.u.							
(III) Theory, room temperature, ambient pressure							
O1	−0.993	−0.726	−0.267	15.621	13.580	2.041	75.7427
C1	0.085	−0.004	0.089	5.940	6.385	−0.445	38.4964
C2	0.388	0.028	0.360	7.096	9.077	−1.981	38.0818
H1	−0.003	0.131	−0.134	7.439	6.832	0.607	0.6520
H2	0.009	0.135	−0.126	6.690	6.085	0.605	0.6488
H3	0.579	0.438	0.141	1.952	3.095	−1.143	0.2931
Molecule	0.004	0.020	−0.016	161.135	161.058	0.077	500.1696
$L_{\rm err}^{\rm molecule}$ = 0.00043 a.u., $L_{\rm err}^{\rm promolecule}$ = 0.00109 a.u., $\Omega_{\rm unit\ cell}/2$ = 161.583 Å^3, $H_e^{\rm Crystal98}$ = −498.5275 a.u.							
(IV) Theory, room temperature, high pressure							
O1	−0.998	−0.723	−0.275	14.671	12.749	1.922	75.5355
C1	0.096	−0.002	0.098	5.784	6.279	−0.495	38.4515
C2	0.383	0.021	0.362	6.960	8.789	−1.829	38.0132
H1	−0.009	0.133	−0.142	6.567	6.040	0.527	0.6578
H2	0.016	0.136	−0.120	5.888	5.327	0.561	0.6435
H3	0.585	0.438	0.147	1.849	2.837	−0.988	0.2848
Molecule	0.005	0.017	−0.012	149.526	149.244	0.282	498.9903
$L_{\rm err}^{\rm molecule}$ = 0.00051 a.u., $L_{\rm err}^{\rm promolecule}$ = 0.00060 a.u., $\Omega_{\rm unit\ cell}/2$ = 149.651 Å^3, $H_e^{\rm Crystal98}$ = −498.5132 a.u.							

$L_{\rm err} = (\Sigma L_\Omega^2/N_{\rm atoms})^{1/2}$, L_Ω is the atomic integrated Lagrangian (Flensburg & Madsen, 2000).

crystal from atoms: when atoms become more negative, their volumes increase and *vice versa*. The sums of the total electronic energies integrated over the atomic basins (Tsirelson & Stash, 2004; Zhurova, Tsirelson, Stash & Pinkerton, 2002) agree with the total energies calculated with wavefunctions using *CRYSTAL*98 within 0.5%. Values of electronic energy per molecule computed both using the *CRYSTAL*98 wavefunction and by means of summing integrated atomic values exhibit the same tendency: they grow slightly with decreasing temperature and increase noticeably for the structure under pressure, correlating well with the corresponding change in the molecular volumes. No significant change in the atomic charges, total or 'deformation', was found.

The non-directional interactions between molecules are often referred to as van der Waals interactions (Katrusiak, 1995). However, based on Feynman's (1939) work, Bader (1998) pointed out that all types of atomic and molecular interactions are mirrored in the electron density, as well as in the negative potential energy density, in the form of the bond-path network. No fundamental distinction between the van der Waals and covalent bond manifestation exists (Slater, 1972); the only distinction consists of the difference in the specific distributions of the electron density, electronic energy density and related characteristics. In particular, the electron density and its curvatures at the CP will be different in value for different types of atomic interactions. In agreement with these observations, we have found several bond paths (Fig. 5) linking the atoms belonging to molecules in neighboring layers as well as between those forming the layers. Characteristics of the intermolecular CPs are also listed in Table 2. The electron density at these CPs is very low and lies within the experimental noise, which was estimated as ~ 0.05 e Å^{-3}. However, the intermolecular CPs are reliably located: their positions, as well as the curvatures of the electron density at the intermolecular bond CPs, are consistent for all four cases studied, both experimental and theoretical. The O1···H1 (Table 2, Fig. 5*a*) interaction can be recognized, essentially, as a weak hydrogen bond. Two symmetry-equivalent H1···H1 bonding interactions (Figs. 2 and 5*b*) are common for all four cases; they are characterized by lower electron density and energy-density values at the CPs compared with the O1···H1 interaction. The O1···H2 interaction with the highest electron-density value between three inter-layer contacts was revealed only for the experimental data and the high-pressure geometry calculation. For the theoretical data at room and low temperatures at ambient pressure, no O1···H2 interaction has been found, but the shorter H2···H2 interaction was revealed instead.[3]

Hydrogen–hydrogen bonding interactions in organic crystals are not uncommon. They have been reported in a number of studies (Matta *et al.*, 2003; Matta, 2006; Robertson *et al.*, 2003; Cortes-Guzman *et al.*, 2003; Zhurova & Pinkerton, 2004), including cases where a H atom bonds to two or more other H atoms (Matta *et al.*, 2003). A significant decrease in the molecular energy due to this interaction has been demonstrated by theoretical calculations (Matta *et al.*, 2003; Matta, 2006). The CPs in the electron density (Table 2), the bond paths (Fig. 5*b*) and additionally located virial paths in the (negative) potential energy density field unambiguously show the bonding character of these interactions in the pentaerythritol crystal.

[3] All these CPs and bond paths also exist in the promolecular electron densities, except for the O1···H1 and O1···H2 interactions at high pressure.

Table 4
Interaction energies (kJ mol^{-1}) for the molecular pairs.

The position of the reference molecule is (0, 0, 0).

	Position of the second molecule	
	(−1, 0, 0)	$(\frac{1}{2}, \frac{1}{2}, \frac{1}{2})$
(II) Theory, low temp., atm. pressure	−31.85	−4.35
(III) theory, room temp., atm. pressure	−32.24	−3.57
(IV) theory, room temp., high pressure	−30.21	−5.60

Interaction energies for molecular pairs have been approximately estimated as the difference between the total energy of a molecular dimer with atomic coordinates as in the crystal and double the energy of a single molecule at the same geometry, both calculated with *CRYSTAL*98 (DFT/B3LYP, 6-311G**) and corrected for the basis-set superposition error.

With an increase of pressure or lowering of temperature, the change in distance between the centers of molecules from neighboring sheets (Table 1) is more than that between the centers of the hydrogen-bonded molecules within the sheets (equal to the unit-cell parameter *a*). This is in line with the Katrusiak (1995) observation that the compressibility of the pentaerythritol crystal along the **c**-axis direction is almost six times larger than along **a** and **b**. The O1···H3 hydrogen bond within the molecular layers becomes 0.013 Å shorter at high pressure compared with ambient pressure (Table 2). Correspondingly, the electron density at the CP is higher by 3.5%, while a ∼7% change in the kinetic and potential energy densities keep the total electronic energy the same. The O1···H3 distance at low temperature is only 0.009 Å longer

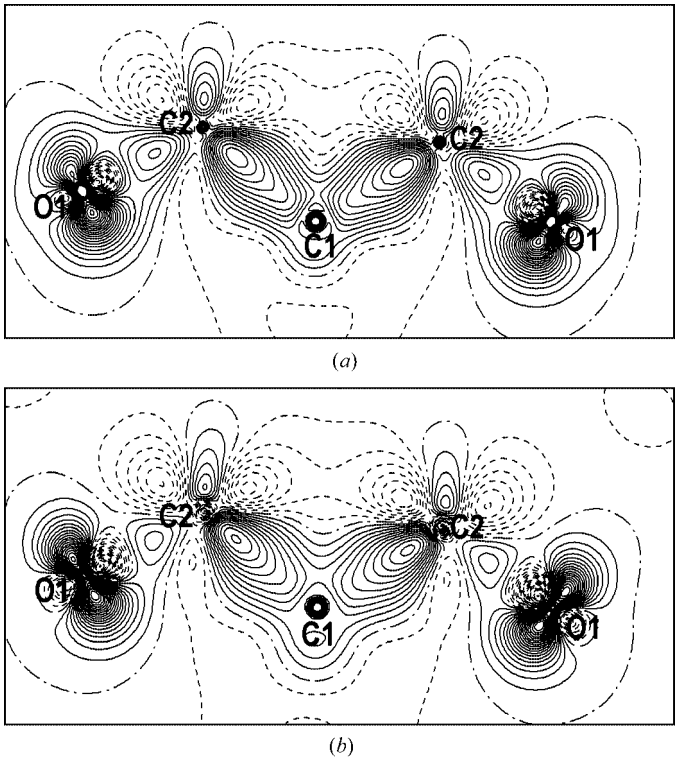

Figure 3
Static deformation density in the C1—O1—C2 plane: (*a*) experimental (I), (*b*) theoretical (IV). Contour interval 0.05 e Å^{-3}. Positive contours are solid, negative contours are dashed and the zero line is dash–dotted.

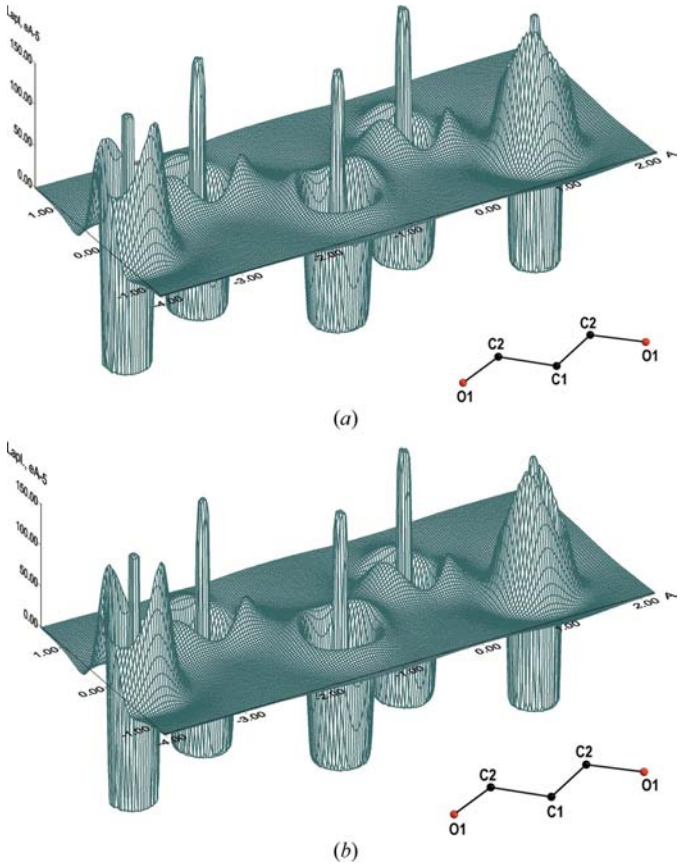

Figure 4
Negative Laplacian of the electron density in the C1—O1—C2 plane: (*a*) experimental (I), (*b*) theoretical (IV). For better visualization, the peaks have been truncated at $\nabla^2 = \pm 150$ e Å^{-5}.

than at room temperature[4] and all the properties of this bond are changed insignificantly. Compression of the unit cell along the *c* axis causes a significant reduction of the O1···H1 and H1···H1 bond lengths; they become 0.221 and 0.125 Å shorter at high pressure, and 0.145 and 0.048 Å shorter at low temperature. The electron-density values at the intermolecular CPs, all the energy-density values, and the dissociation energies are much larger at high pressure and low temperature compared with the room-temperature and normal-pressure cases (Table 2); this effect is more pronounced for the O1···H1 than for the H1···H1 interaction.

Espinosa & Molins (2000) have found that the electronic energy density at the CP is linearly related to the pairwise interaction potential. They also indicated that the change in the potential interaction energy (ΔU), induced by temperature or pressure, is proportional to the difference in the local potential energy values at these CPs. However, it appears that the interlayer interactions in this crystal are not described correctly by the superposition of the pairwise potentials. At

[4] The O1···H3 distance at low temperature becomes slightly longer due to the relative increase of the unit-cell parameter *a*. After comparing several sources of the PE crystal structure at ambient conditions (Llewellyn *et al.*, 1937; Ladd, 1979; Eilerman & Rudman, 1979; Semmingsen, 1988), we consider this increase to be insignificant.

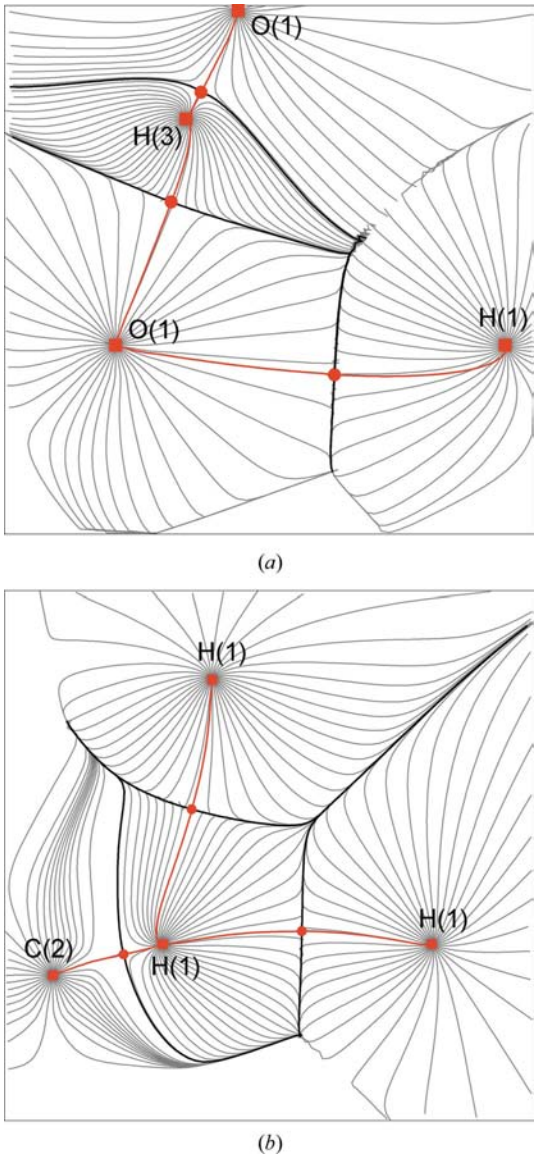

Figure 5
Gradient paths in the electron density: (*a*) O1—H3···H1 plane, experimental data; the O1···H1, O1—H3 and H3···O1 bond paths are shown; (*b*) H1···H1···H1 plane, high-pressure (theoretical) data, two symmetry-equivalent H1···H1 bond paths are shown. (3,−3) critical points (maxima) are shown as red squares, (3,−1) bond critical points are red circles, bond paths are red lines and projections of atomic zero-flux surfaces are shown as black lines. See also Fig. 2.

the same time, we can note that the profile of the total electronic energy density, $h_e(\mathbf{r})$, along the O1···H3 bond line (Fig. 6) is quite sharp, whereas that for the O1···H1 interaction between the molecular layers is relatively flat. This correlates well with the larger compressibility of the pentaerythritol crystal along the **c**-axis direction mentioned above.

Intermolecular interaction energies between nearest molecules within the molecular layers are much larger than those between the nearest molecules of different molecular layers (Table 4). With respect to room temperature, the unit-cell parameter *a* becomes insignificantly longer at low temperature (by 0.1%) and shorter at high pressure (by 1%, Table 1). The intermolecular energy of a pair of molecules at (0,0,0) and (−1,0,0) becomes less negative at low temperature and high pressure, as expected because of the increase in the intermolecular repulsive forces within the molecular layers. The unit-cell parameter *c* is much shorter at low temperature (by 3%) and high pressure (by 6%), but the intermolecular energies of a pair of molecules at (0,0,0) and $(\frac{1}{2},\frac{1}{2},\frac{1}{2})$ become more negative showing that the interaction becomes stronger, as is also seen from the $h_e(\mathbf{r})$ plot (Fig. 6*b*). The energy

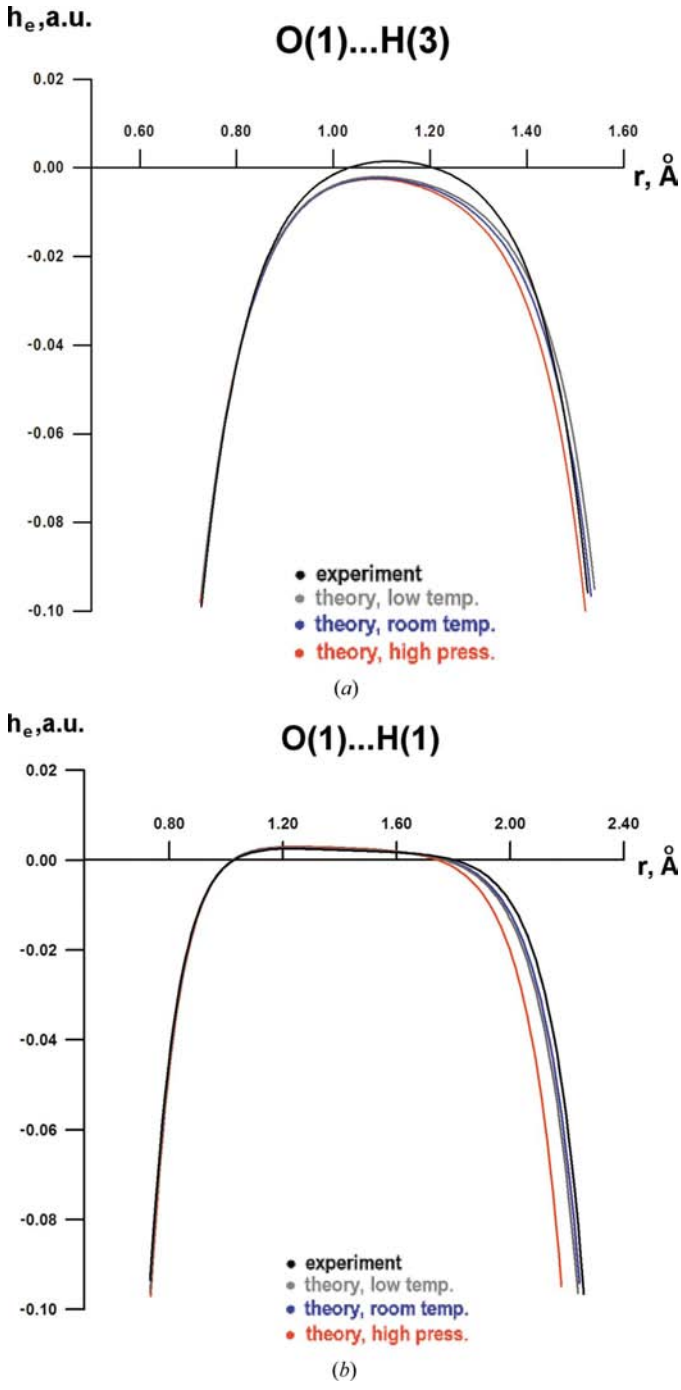

Figure 6
Electronic energy density (*a*) along the O1···H3 line (hydrogen bond within molecular layers) and (*b*) along the O1···H1 line (hydrogen bond between molecular layers). The O atom was placed at $r = 0$ and the corresponding hydrogen is located at the appropriate distance (Table 2).

densities at the appropriate critical points (Table 2) reflect exactly the same picture. Thus, the total description of the interaction is a result of many competing factors: we can thus suppose that the specific nature of the intermolecular interaction potential between the molecular layers, which is reflected in its flatness, is responsible for the observed small increase in the interaction between the layers.

In conclusion, the most significant changes in the pentaerythritol crystal due to lowering the temperature or increasing the pressure take place in the intermolecular areas, mainly along the **c** axis. The molecular layers become closer at low temperature or high pressure, resulting in an increase in the interaction between the layers. The latter manifests itself in more negative intermolecular energies, higher electron density, energy densities and dissociation energy at the corresponding CPs and sharper electronic energy-density profiles. In contrast, the intermolecular interactions within the molecular layers become weaker, as expected owing to the increase in repulsive forces.

The financial support of the Office of Naval Research through the contract number N00014-05–1-0397 is gratefully appreciated. V.G.T. and A.I.S. thank the Russian Federal Agency for Education for financial support within the frameworks of Program 'Development of the Highest-School Scientific Potential: 2006–2008' (subsection 2.1.1). We thank the referees for valuable comments.

References

Abramov, Y. A. (1997). *Acta Cryst.* A**53**, 264–272.
Bader, R. F. W. (1990). *Atoms in Molecules: A Quantum Theory. The International Series of Monographs of Chemistry*, edited by J. Halpen & M. L. H. Green, pp. 1–438. Oxford: Clarendon Press.
Bader, R. W. F. (1998). *J. Phys. Chem. A*, **102**, 7314–7323.
Cortes-Guzman, F., Hernandez-Trujillo, J. & Cuevas, G. (2003). *J. Phys. Chem.* **107**, 9253–9256.
Eilerman, D. & Rudman, R. (1979). *Acta Cryst.* B**35**, 2458–2460.
Espinosa, E., Lecomte, C. & Molins, E. (1999). *Chem. Phys. Lett.* **300**, 745–748.
Espinosa, E. & Molins, E. (2000). *J. Chem. Phys.* **11**, 5686–5694.
Espinosa, E., Molins, E. & Lecomte, C. (1998). *Chem. Phys. Lett.* **285**, 170–173.
Feynman, R. (1939). *Phys. Rev.* **56**, 340–343.
Flensburg, C. & Madsen, D. (2000). *Acta Cryst.* A**56**, 24–28.
Gracia, L., Marques, M., Beltran, A., Martin Pendas, A. & Recio, J. M. (2004). *J. Phys. Condens. Matter*, **16**, S1263–S1270.
Hansen, N. & Coppens, P. (1978). *Acta Cryst.* A**34**, 909–921.
Hardie, M. J., Kirschbaum, K., Martin, A. & Pinkerton, A. A. (1998). *J. Appl. Cryst.* **31**, 815–817.
Katrusiak, A. (1995). *Acta Cryst.* B**51**, 873–879.
Kirschbaum, K., Martin, A., Parrish, D. & Pinkerton, A. A. (1999). *J. Phys. Condens. Matter*, **11**, 4483–4490.
Kirzhnits, D. A. (1957). *Sov. Phys. JETP*, **5**, 64–71.
Koritsanszky, T., Richter, T., Macci, P., Gatti, C., Howard, S., Mallinson, P. R., Farrugia, L., Su, Z. W. & Hansen, N. K. (2003). *XD*. Technical Report. Freie Universität Berlin, Berlin, Germany.
Ladd, M. F. (1979). *Acta Cryst.* B**35**, 2375–2377.
Llewellyn, F. J., Cox, E. G. & Goodwin, T. H. (1937). *J. Chem. Soc.* Abstr., pp. 883–894.
Maslen, E. N. & Spackman, M. A. (1985). *Aust. J. Phys.* **38**, 273–287.
Matta, C. F. (2006). *Hydrogen Bonding – New Insight (Challenges and Advances in Computational Chemistry and Physics Series*), edited by S. Grabowski. Dordrecht: Kluwer Academic Publishers. In the press.
Matta, C. F., Hernandez-Trujillo, J., Tang, T.-H. & Bader, R. F. W. (2003). *Chem. Eur. J.* **9**, 1940–1951.
Pinkerton, A. A., Zhurova, E. A. & Chen, Y.-S. (2003). *Energetic Materials*, Part 1, *Decomposition, Crystal and Molecular Properties, Theoretical and Computational Chemistry*, Vol. 12, pp. 215–245. Amsterdam: Elsevier Science Ltd.
Ribaud, L., Wu, G., Zhang, Y. & Coppens, P. (2001). *J. Appl. Cryst.* **34**, 76–79.
Ritchie, J. P., Zhurova, E. A., Martin, A. & Pinkerton, A. A. (2003). *J. Phys. Chem. B*, **107**, 14576–14589.
Robertson, K. N., Knop, O. & Cameron, T. S. (2003). *Can. J. Chem.* **81**, 727–743.
Saunders, V. R., Dovesi, R., Roetti, C., Causà, M., Harrison, N. M., Orlando, R. & Zicovich-Wilson, C. M. (1998). *CRYSTAL*98 *User's Manual.* University of Torino, Italy.
Semmingsen, D. (1988). *Acta Chem. Scand. A*, **42**, 279–283.
Slater, J. C. (1972). *J. Chem. Phys.* **57**, 2390–2396.
Stash, A. I. & Tsirelson, V. G. (2002). *J. Appl. Cryst.* **35**, 371–373.
Stash, A. I. & Tsirelson, V. G. (2005). *Crystallogr. Rep.* **50**, 202–209.
Tsirelson, V. G. (2002). *Acta Cryst.* B**58**, 632–639.
Tsirelson, V. G. & Stash, A. I. (2004). *Acta Cryst.* A**60**, 418–426.
Zhurov, V. V., Zhurova, E. A., Chen, Y.-S. & Pinkerton, A. A. (2005). *J. Appl. Cryst.* **38**, 827–829.
Zhurova, E. A., Martin, A. & Pinkerton, A. A. (2002). *J. Am. Chem. Soc.* **124**, 8741–8750.
Zhurova, E. A. & Pinkerton, A. A. (2001). *Acta Cryst.* B**57**, 359–365.
Zhurova, E. A. & Pinkerton, A. A. (2004). Unpublished data for biguanidinium dinitramides and estrone.
Zhurova, E. A., Tsirelson, V. G., Stash, A. I. & Pinkerton, A. A. (2002). *J. Am. Chem. Soc.* **124**, 4574–4575.
Zhurova, E. A., Tsirelson, V. G., Stash, A. I., Yakovlev, M. V. & Pinkerton, A. A. (2004). *J. Phys. Chem. B*, **108**, 20173–20179.